AFRL-AFOSR-VA-TR-2020-0040

Non-linear growth and breakdown toward turbulence in Hypersonic Boundary layers: Investigation of fundamental physical mechanisms

Sharath Girimaji
TEXAS ENGINEERING EXPERIMENT STATION COLLEGE STATION

11/14/2019
Final Report

Air Force Research Laboratory
AF Office Of Scientific Research (AFOSR)/ RTA1
Arlington, Virginia 22203
Air Force Materiel Command

REPORT DOCUMENTATION PAGE

Form Approved
OMB No. 0704-0188

1. REPORT DATE *(DD-MM-YYYY)*	2. REPORT TYPE	3. DATES COVERED *(From - To)*
16-03-2020	Final Performance	15 Aug 2016 to 14 Aug 2019

4. TITLE AND SUBTITLE
Non-linear growth and breakdown toward turbulence in Hypersonic Boundary layers: Investigation of fundamental physical mechanisms

5a. CONTRACT NUMBER

5b. GRANT NUMBER
FA9550-16-1-0360

5c. PROGRAM ELEMENT NUMBER
61102F

6. AUTHOR(S)
Sharath Girimaji

5d. PROJECT NUMBER

5e. TASK NUMBER

5f. WORK UNIT NUMBER

7. PERFORMING ORGANIZATION NAME(S) AND ADDRESS(ES)
TEXAS ENGINEERING EXPERIMENT STATION COLLEGE STATION
1470 WILLIAM D FITCH PKY
COLLEGE STATION, TX 77843-3577 US

8. PERFORMING ORGANIZATION REPORT NUMBER

9. SPONSORING/MONITORING AGENCY NAME(S) AND ADDRESS(ES)
AF Office of Scientific Research
875 N. Randolph St. Room 3112
Arlington, VA 22203

10. SPONSOR/MONITOR'S ACRONYM(S)
AFRL/AFOSR RTA1

11. SPONSOR/MONITOR'S REPORT NUMBER(S)
AFRL-AFOSR-VA-TR-2020-0040

12. DISTRIBUTION/AVAILABILITY STATEMENT
A DISTRIBUTION UNLIMITED: PB Public Release

13. SUPPLEMENTARY NOTES

14. ABSTRACT

The work performed under this grant addresses two important aspects that affect accurate computation and prediction of transition to turbulence in hypersonic boundary layers: (i) the non-linear breakdown toward turbulence physics is not well understood in hypersonic boundary layers; and (ii) computational methods based directly on gas kinetic theory have not been as well developed, despite their inherent advantages for computing hypersonic flows. Three studies are performed to address the above gaps in the current state of the art. In the first study, critical mathematical framework to analyze and understand the non-linear internal-kinetic energy interactions and subsequent spectral energy transfer is developed. This development is the first of its kind to clearly identify and explain the interchange between the mean and fluctuating fields of internal and kinetic energy. The second study develops and validates a promising gas kinetic scheme (GKS) for high-speed wall bounded flows. Validation studies are performed in flows ranging from subsonic speeds to convective Mach number of about 6. The scheme and code are validated against benchmark data and linear theory results. The accuracy of the solver for capturing non-linear physics is also well established. The third study examines perturbation growth and non-linear breakdown to transition at various speeds. The contrast between incompressible flow and hypersonic flow non-linear breakdown physics is well established. It is shown that kinetic-internal energy exchange can lead to significant slow down in the transfer of energy from large to small scales. In turn, this can delay the onset of breakdown in high speed flows. Overall, the studies performed under this proposal, lead to valuable advances in our ability to compute and predict the transition phenomenon in hypersonic boundary layers.

15. SUBJECT TERMS
DNS, Initial Value Problem (IVP), Non-linear breakdown

Standard Form 298 (Rev. 8/98)
Prescribed by ANSI Std. Z39.18

16. SECURITY CLASSIFICATION OF:			17. LIMITATION OF ABSTRACT	18. NUMBER OF PAGES	19a. NAME OF RESPONSIBLE PERSON
a. REPORT	b. ABSTRACT	c. THIS PAGE			LEYVA, IVETT
Unclassified	Unclassified	Unclassified	UU		19b. TELEPHONE NUMBER *(Include area code)* 703-696-8478

Standard Form 298 (Rev. 8/98)
Prescribed by ANSI Std. Z39.18

Final Performance Report

Nonlinear growth and breakdown towards turbulence in Hypersonic Boundary layers

AFOSR Grant FA9550-16-1-0360

Sharath S. Girimaji
Texas A&M University

November 14, 2019

ABSTRACT

The work performed under this grant addresses two important aspects that affect accurate computation and prediction of transition to turbulence in hypersonic boundary layers: (i) the non-linear breakdown toward turbulence physics is not well understood in hypersonic boundary layers; and (ii) computational methods based directly on gas kinetic theory have not been as well developed, despite their inherent advantages for computing hypersonic flows. Three studies are performed to address the above gaps in the current state of the art. In the first study, critical mathematical framework to analyze and understand the non-linear internal-kinetic energy interactions and subsequent spectral energy transfer is developed. The second study develops and validates a promising gas kinetic scheme (GKS) for high-speed wall bounded flows. Validation studies are performed in flows ranging from subsonic speeds to convective Mach number of about 6. The scheme and code are validated against benchmark data and linear theory results. The third study examines perturbation growth and non-linear breakdown to transition at various speeds. The contrast between incompressible flow and hypersonic flow non-linear breakdown physics is well established. Overall, the studies performed under this proposal, lead to valuable advances in our ability to compute and predict the transition phenomenon in hypersonic boundary layers.

1 Introduction

Much progress has been made in recent years toward understanding, modeling and predicting transition and turbulence processes in hypersonic boundary layers. Two areas in which there are significant deficiencies and more efforts are needed are (i) Understanding the non-linear processes in the breakdown toward turbulence; and (ii) Development of appropriate numerical schemes and tools based on Gas Kinetic Theory that are more appropriate for high-speed flows than Navier-Stokes equations. This work addresses these two areas of importance for predictive simulations of hypersonic transition in flows of interest to Air Force.

The first objective of this work is to investigate the key non-linear processes occurring during the early stages of breakdown toward turbulence in hypersonic boundary layers. Specifically, we seek to contrast the non-linear breakdown physics in incompressible and compressible flows. The focus is on pressure-related non-linear processes. This is due to the fact that there is a fundamental change in the character of pressure from low to high Mach numbers. While much effort has been expended on linear stability theories for compressible flows, a corresponding effort in understanding non-linear effects have been lacking. One key factor that renders non-linear effects different in compressible flows is the emergence of dilatational field and internal energy fluctuations. In incompressible transition, perturbation kinetic energy grows and cascades to smaller scales leading to 'de-correlation' of the flow field and turbulence. However, at high speeds, perturbation kinetic energy can be converted into internal energy of the mean flow or fluctuations. Thus, the perturbation energy available for breakdown to small scales can be significantly lower. The canonical incompressible non-linear spectral transfer is profoundly modified at hypersonic speeds. Despite this critical change in the character of non-linear process, the underlying physics of the phenomenon has not been investigated in the past. There is a compelling need to understand the non-linear kinetic-internal energy interactions and spectral growth in hypersonic boundary layers.

The second aspect of the work is the development of a Gas Kinetic Scheme (GKS) to compute transition and turbulence in hypersonic flows. At the current stage, most of the hypersonic flow computations are still being performed with compressible Navier-Stokes solvers with modifications to account for various high-speed, high-enthalpy effects. While such solvers are adequate, at hypersonic flow conditions, there are tremendous advantages to using numerical schemes based on the more fundamental Boltzmann equation.

Toward the above objectives, three studies were undertaken.

1. Study 1 develops the fundamental framework and governing equations needed to analyze internal energy interactions and its spectral distribution in a manner similar to that of kinetic energy analysis. To emulate the role of velocity in kinetic energy analysis, a new variable ($\phi \sim \sqrt{p}$ where p is pressure) is introduced to enable the examination of internal energy dynamics. Evolution equations for the mean and fluctuating components of ϕ are

derived. These equations enable precise examination of mean–turbulent flow internal energy interactions, internal–kinetic energy exchange and spectral distribution of internal energy.

2. Study 2 focuses on the compressible linear stability theory (CLST) to determine the most unstable modes at different Mach numbers. Linearized perturbation equations are derived and an eigenvalue analysis is performed. A code is developed to solve for the most unstable mode and its shape. DNS with randomly perturbed pressure field are performed and the most unstable mode and mode shapes are compared with CLST for verification of linear analysis code. The verified linear analysis code enables the study of Mach number effects on the stability of low wavenumbers and reaffirms the relevance of the effective gradient Mach number, M_g^e.

3. Study 3 characterizes the nonlinear evolution of perturbations in high Mach number Poiseuille flow and contrasts the behavior against equivalent incompressible flow. The focus is on the effect of changing nature of pressure (with Mach number) on three crucial processes: (i) internal energy evolution; (ii) kinetic-internal energy exchange; and (iii) evolution of kinetic energy spectrum. We perform direct numerical simulations of plane Poiseuille flow at different Mach numbers subject to a variety of initial perturbations. In all high-speed cases considered, pressure dilatation leads to energy equipartition between wall-normal velocity fluctuations (dilatational kinetic energy) and pressure fluctuations (a measure of internal energy). However, the effect of pressure-dilatation on kinetic energy spectral growth can be varied. In cases wherein pressure-dilatation is larger than turbulent kinetic energy production, spectral growth is considerably slower than in equivalent low Mach number case. When pressure-dilatation is smaller than production, the spectral growth is only marginally affected. As a consequence, in high-speed Poiseuille flow the spectral growth rate varies with wall-normal distance depending on the local pressure effects. These findings provide valuable insight into the nonlinear aspects of breakdown towards turbulence in high speed wall-bounded shear flows.

2 Study 1: Internal-Kinetic Energy Interactions and Spectral Energy Transfer

2.1 Introduction

Kinetic energy dynamics such as inter-scale transfer and spectral distribution are key features of turbulence and have been the subject of several investigations over many decades. In incompressible flows, wherein density is constant and uniform, the velocity (u_i) evolution equation, Navier-Stokes or the momentum conservation equation, forms the basis of kinetic energy analysis.

For example, scale-to-scale energy transfer characteristics are dictated by the triadic interactions incumbent in the advective term of the spectral Navier-Stokes equation. The kinetic energy spectrum is computed from Fourier-transforming the auto-covariance function of the velocity field.

The advent of compressibility renders the kinetic energy dynamics more complicated due to two factors: (i) spatio-temporal variations in density; and (ii) interactions with internal energy. Some of the complexities in kinetic energy dynamics due to density variations can be adequately addressed by considering density-weighted velocity field – ρu_i leading to Favre-averaging. But investigation of scale-to-scale transfer and spectral distribution require additional considerations. A new variable $\sqrt{\rho}u_i$, first proposed by Kida and Orszag (1992), has been utilized in many works for computing kinetic energy spectrum in compressible turbulence.

The focus of this study is on the investigation of internal energy dynamics and its interaction with kinetic energy. It is desirable to investigate and characterize internal energy interactions in turbulence in a manner similar to that of kinetic energy analysis. Many studies perform insightful investigations of turbulent fluctuations of pressure. However, such studies do not address internal energy spectral distribution or transfer in a manner similar to that of kinetic energy. For example, the scale-to-scale transfer of internal energy cannot be computed from the advection term in the spectral pressure equation. Further, the turbulent internal energy spectrum is not the same as the turbulent pressure spectrum. To overcome these limitations, Miura and Kida (1995) propose a new internal energy variable ($\phi \sim \sqrt{p}$) corresponding to velocity for investigating the internal energy spectrum.

The objective is to extend the proposal of Miura and Kida and develop the mathematical framework and evolution equations required for performing a comprehensive and rigorous analysis of turbulent internal energy dynamics based on ϕ. Similar to kinetic energy analysis, we aim at partitioning the internal energy into two parts corresponding to contribution of the mean field and the fluctuating field. The equations based on ϕ will enable rigorous investigations of (i) internal–kinetic energy interactions at each scale; (ii) mean–turbulent internal energy exchange; and (iii) spectral distribution of internal and total energies in a turbulent flow field. The proposed framework is very important for a comprehensive understanding of total energy dynamics and spectral energy distribution in high-speed, compressible transition and turbulent flows.

2.2 Governing Equations

The compressible Navier-Stokes equations for a calorically perfect ideal gas form the basis of this analysis:

$$\frac{\partial \rho}{\partial t} + \frac{\partial}{\partial x_j}(\rho u_j) = 0, \tag{1a}$$

$$\frac{\partial (\rho u_i)}{\partial t} + \frac{\partial (\rho u_i u_j)}{\partial x_j} = -\frac{\partial p}{\partial x_i} + \frac{\partial \tau_{ij}}{\partial x_j}, \tag{1b}$$

$$\frac{\partial}{\partial t}\Big(\frac{p}{\gamma - 1}\Big) + \frac{\partial}{\partial x_j}\Big(\frac{p u_j}{\gamma - 1}\Big) = \frac{\partial}{\partial x_j}\Big(\kappa \frac{\partial T}{\partial x_j}\Big) - p\frac{\partial u_k}{\partial x_k} + \tau_{ij}\frac{\partial u_i}{\partial x_j}, \tag{1c}$$

$$p = \rho R T, \tag{1d}$$

where ρ is the fluid density, u_i is velocity component, τ_{ij} is the viscous stress tensor, p is the gas pressure, γ is ratio of specific heats at constant pressure and volume, κ is the coefficient of thermal conductivity, T is the temperature, x_i is the spatial coordinate and t is time. The viscous stress tensor is given by:

$$\tau_{ij} = \mu\Big(\frac{\partial u_i}{\partial x_j} + \frac{\partial u_j}{\partial x_i}\Big) + \lambda \frac{\partial u_k}{\partial x_k}\delta_{ij}, \tag{2}$$

where μ is the coefficient of dynamic viscosity, λ is the coefficient of second viscosity and δ_{ij} is the Kronecker delta.

Nonlinear evolution of perturbations is highly dependent on interactions between kinetic and internal energies. We first analyze the kinetic (K), internal (e) and total (E) energy equations to identify the key interactions:

$$\frac{\partial K}{\partial t} + \frac{\partial (K u_k)}{\partial x_k} + \frac{\partial}{\partial x_k}\Big[p u_k - \tau_{ik} u_i\Big] = p\frac{\partial u_k}{\partial x_k} - \tau_{ij}\frac{\partial u_i}{\partial x_j}, \tag{3a}$$

$$\frac{\partial e}{\partial t} + \frac{\partial (e u_k)}{\partial x_k} + \frac{\partial q_k}{\partial x_k} = -p\frac{\partial u_k}{\partial x_k} + \tau_{ij}\frac{\partial u_i}{\partial x_j}, \tag{3b}$$

$$\frac{\partial E}{\partial t} + \frac{\partial (E u_k)}{\partial x_k} + \frac{\partial}{\partial x_k}\Big[p u_k - \tau_{ik} u_i + q_k\Big] = 0, \tag{3c}$$

where,

$$K = \frac{1}{2}\rho u_i u_i, \quad e = \frac{p}{\gamma - 1}, \quad q_k = -\kappa\frac{\partial T}{\partial x_k} \quad \text{and} \quad E = K + e. \tag{4}$$

Equations (3a) and (3b) indicate interactions between kinetic and internal energy via pressure-dilatation and viscous action. Pressure-dilatation permits a two-way exchange while viscous action can only lead to a one-way transfer from kinetic to internal energy.

2.3 Framework Development and Energy Interactions

It is important to recognize that the mean kinetic energy of the flow has two contributions: the kinetic energy associated with the mean flow field and that associated with the fluctuations.

$$\overline{K} = K_m + k \quad \text{where,} \quad K_m = \frac{1}{2}\overline{\rho}\tilde{U}_i\tilde{U}_i \quad \text{and} \quad k = \frac{1}{2}\overline{\rho u_i'' u_i''}. \tag{5}$$

where $\tilde{U}_i$ a Favre averaged velocity and u_i'' is the corresponding fluctuation field.

Governing equation for K_m and k are well known and can be written as:

$$\begin{aligned}\frac{\partial K_m}{\partial t} + \frac{\partial (K_m \tilde{U}_j)}{\partial x_j} + \frac{\partial}{\partial x_j}\left[\overline{\rho u_i'' u_j''}\tilde{U}_i + \overline{p}\,\overline{U}_j - \overline{\tau_{ij}}\,\overline{U}_i\right] = &\overline{\rho u_i'' u_j''}\frac{\partial \tilde{U}_i}{\partial x_j} + \overline{p}\frac{\partial \overline{U}_k}{\partial x_k} \\ &- \overline{\tau_{ij}}\frac{\partial \overline{U}_i}{\partial x_j} + \overline{u_k''}\frac{\partial \overline{p}}{\partial x_k} - \overline{u_k''}\frac{\partial \overline{\tau_{kj}}}{\partial x_j},\end{aligned} \tag{6}$$

and

$$\begin{aligned}\frac{\partial k}{\partial t} + \frac{\partial (k\tilde{U}_j)}{\partial x_j} + \frac{\partial}{\partial x_j}\left[\frac{1}{2}\overline{\rho u_i'' u_i'' u_j''} + \overline{p' u_j'} - \overline{\tau_{ij}' u_i'}\right] = &-\overline{\rho u_i'' u_j''}\frac{\partial \tilde{U}_i}{\partial x_j} + \overline{p'\frac{\partial u_k'}{\partial x_k}} \\ &- \overline{\tau_{ij}'\frac{\partial u_i'}{\partial x_j}} - \overline{u_k''}\frac{\partial \overline{p}}{\partial x_k} + \overline{u_k''}\frac{\partial \overline{\tau_{kj}}}{\partial x_j}.\end{aligned} \tag{7}$$

In incompressible flows, the spectral transfer and distribution of kinetic energy across different scales of motion can be examined by performing Fourier transform of u_i'. However, Fourier transform of u_i'' alone is not enough for scale-to-scale analysis of compressible flows. As proposed by Kida and Orszag (1992), similar spectral energy analysis of compressible flows requires a new variable,

$$w_i = \sqrt{\rho}\, u_i'', \tag{8}$$

to account for spatio-temporal variations in density. The Fourier transform of the auto-correlation function of w_i yields the kinetic energy spectrum. The quartic interactions for turbulent kinetic energy cascade are also reduced to triadic interactions.

Unlike kinetic energy, it is more complicated to clearly identify the internal energy associated with the mean (or background field) and the turbulent internal energy. In the linear regime, when the density fluctuations are small, Sarkar (1991) identified that the potential energy incumbent in pressure fluctuations can be approximated as $\overline{p'p'}/(2\gamma\overline{p})$. However, this representation is inadequate when the density fluctuations are large. Miura and Kida (1995) propose a more general approach which is valid for strongly compressible flows. They propose a new variable,

$$\phi \equiv \sqrt{e} = \sqrt{\frac{p}{\gamma - 1}}, \tag{9}$$

for examining the internal energy spectrum in simple isotropic flows. The justification is that ϕ^2 corresponds to internal energy. Using the relation $\gamma p = \rho a^2$, where a is the speed of sound, ϕ can be written as:

$$\phi = \frac{1}{\sqrt{\gamma(\gamma-1)}}\sqrt{\rho}a. \tag{10}$$

Eq. (10) shows that ϕ includes density-weighted acoustic speed information which relates to the internal energy of the system. The state variable ϕ for internal energy is thus analogous to w_i for turbulent kinetic energy. ϕ can now be decomposed using Reynolds averaging:

$$\phi = \overline{\phi} + \phi' \;\text{ where, }\; \overline{\phi} = \overline{\sqrt{\frac{p}{\gamma-1}}} \;\text{ and }\; \phi' = \sqrt{\frac{p}{\gamma-1}} - \overline{\sqrt{\frac{p}{\gamma-1}}}. \tag{11}$$

With this formulation, it is possible to clearly separate the mean internal energy of the flow into a mean field and a fluctuating field contribution,

$$\overline{e} = \overline{\phi^2} = \overline{\phi}\,\overline{\phi} + \overline{\phi'\phi'} \quad \text{therefore,} \quad e_m = \overline{\phi}\,\overline{\phi} \quad \text{and} \quad e_t = \overline{\phi'\phi'}. \tag{12}$$

The strong similarity of internal energy decomposition in eq. (12) and kinetic energy partitioning in eq. (5) is clearly evident. The spectral transfer and spectral distribution of turbulent internal energy can be characterized from the behavior ϕ' much in the same manner as the turbulent kinetic energy transfer/distribution can be analyzed using $w_i = \sqrt{\rho}u_i''$. The Fourier transform of the auto-correlation of ϕ' yields the turbulent internal energy spectrum. Thus, $\phi' - w_i$ interactions hold the key to examining internal–kinetic energy exchange.

The mean and the fluctuation pressure field can be written in terms of the internal energy velocity variable ϕ as:

$$\overline{p} = (\gamma-1)\left[\overline{\phi}\,\overline{\phi} + \overline{\phi'\phi'}\right] \quad \text{and} \quad p' = (\gamma-1)\left[\phi'\phi' + 2\overline{\phi}\phi' - \overline{\phi'\phi'}\right]. \tag{13}$$

We can clearly see that mean and fluctuating pressure have a linear and nonlinear component:

$$\overline{p} = \overline{p}_m + \overline{p}_t \quad \text{and} \quad p' = p'_m + p'_t \tag{14}$$

where,

$$\begin{aligned} \overline{p}_m &= (\gamma-1)\overline{\phi}\,\overline{\phi} \quad \text{and} \quad \overline{p}_t = (\gamma-1)\overline{\phi'\phi'}, \\ p'_m &= 2(\gamma-1)\overline{\phi}\phi' \quad \text{and} \quad p'_t = (\gamma-1)\left[\phi'\phi' - \overline{\phi'\phi'}\right]. \end{aligned} \tag{15}$$

Here, $\overline{p}_m$ and $\overline{p}_t$ are the components of mean pressure associated with the mean field and the perturbation field respectively. Similarly, p'_m and p'_t are the components of fluctuating pressure associated with the mean field and the perturbation field. $\overline{p}_m$ and p'_m can also be understood as

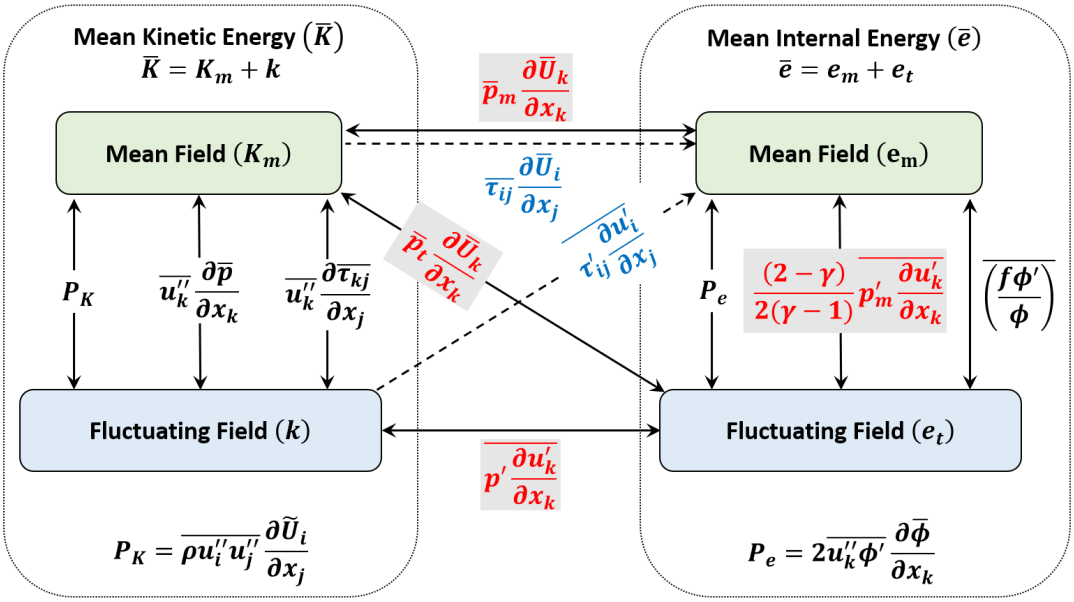

Figure 1: Interactions between kinetic and internal energies in the nonlinear regime using eqs. (6,7,17b,17d)

linear (or rapid) components while $\overline{p}_t$ and p'_t as nonlinear (or slow) components.

We can now derive the evolution equations for $e_m = \overline{\phi}\,\overline{\phi}$ and $e_t = \overline{\phi'\phi'}$. We start with the internal energy equation, eq. (3b) and use definitions $e = \phi^2$ and $p = (\gamma-1)\phi^2$ to obtain an equation for ϕ:

$$\frac{\partial \phi}{\partial t} + u_k \frac{\partial \phi}{\partial x_k} = -\frac{\gamma}{2}\phi \frac{\partial u_k}{\partial x_k} + \frac{f}{2\phi} \quad \text{where,} \quad f = \left[-\frac{\partial q_k}{\partial x_k} + \tau_{ij} \frac{\partial u_i}{\partial x_j} \right]. \tag{16}$$

The governing equations for $\overline{\phi}$, e_m, ϕ' and e_t can now be expressed as:

$$\frac{\partial \overline{\phi}}{\partial t} + \tilde{U}_k \frac{\partial \overline{\phi}}{\partial x_k} + \overline{u''_k} \frac{\partial \overline{\phi}}{\partial x_k} + \overline{u''_k \frac{\partial \phi'}{\partial x_k}} = -\frac{\gamma}{2}\left[\overline{\phi} \frac{\partial \tilde{U}_k}{\partial x_k} + \overline{\phi} \frac{\partial \overline{u''_k}}{\partial x_k} + \overline{\phi' \frac{\partial u''_k}{\partial x_k}} \right] + \frac{\overline{f}}{2\overline{\phi}} - \frac{1}{2\overline{\phi}} \overline{\left(\frac{f\phi'}{\phi} \right)}. \tag{17a}$$

$$\begin{aligned} \frac{\partial e_m}{\partial t} + \frac{\partial (e_m \tilde{U}_k)}{\partial x_k} + \frac{\partial}{\partial x_k}\left[\overline{\phi}\,\overline{\phi}\,\overline{u''_k} + 2\overline{\phi}\,\overline{\phi' u''_k} + \overline{q_k} \right] = {} & \overline{\tau_{ij}} \frac{\partial \overline{U}_i}{\partial x_j} + \overline{\tau'_{ij} \frac{\partial u'_i}{\partial x_j}} - \overline{p}_m \frac{\partial \overline{U}_k}{\partial x_k} \\ & + 2\overline{u''_k \phi'} \frac{\partial \overline{\phi}}{\partial x_k} + \frac{(2-\gamma)}{2(\gamma-1)} \overline{p'_m \frac{\partial u'_k}{\partial x_k}} - \overline{\left(\frac{f\phi'}{\phi} \right)}. \end{aligned} \tag{17b}$$

$$\begin{aligned} \frac{\partial \phi'}{\partial t} + \tilde{U}_k \frac{\partial \phi'}{\partial x_k} + u''_k \frac{\partial \overline{\phi}}{\partial x_k} + u''_k \frac{\partial \phi'}{\partial x_k} - \overline{u''_k} \frac{\partial \overline{\phi}}{\partial x_k} - \overline{u''_k \frac{\partial \phi'}{\partial x_k}} = {} & -\frac{\gamma}{2}\left[\phi' \frac{\partial \tilde{U}_k}{\partial x_k} + \overline{\phi} \frac{\partial u''_k}{\partial x_k} + \phi' \frac{\partial u''_k}{\partial x_k} - \overline{\phi} \frac{\partial \overline{u''_k}}{\partial x_k} - \overline{\phi' \frac{\partial u''_k}{\partial x_k}} \right] \\ & + \left(\frac{f}{2\phi} \right)'. \end{aligned} \tag{17c}$$

$$\frac{\partial e_t}{\partial t} + \frac{\partial (e_t \tilde{U}_k)}{\partial x_k} + \frac{\partial}{\partial x_k}[\overline{\phi'\phi' u''_k}] = -\overline{p}_t \frac{\partial \overline{U}_k}{\partial x_k} - \overline{p' \frac{\partial u'_k}{\partial x_k}} - 2\overline{u''_k \phi'} \frac{\partial \overline{\phi}}{\partial x_k} - \frac{(2-\gamma)}{2(\gamma-1)} \overline{p'_m \frac{\partial u'_k}{\partial x_k}} + \overline{\left(\frac{f\phi'}{\phi} \right)}. \tag{17d}$$

The equations for $\overline{\phi}$, e_m, ϕ' and e_t in eqs. (17a), (17b), (17c) and (17d) constitute the framework required to describe internal energy interactions. The kinetic–internal energy interactions specifically the energy exchanges amongst K_m, k, e_m and e_t are summarized in figure 1. The double solid arrow represents a two-way exchange while a dashed one-way arrow represents a single sided transfer of energy.

2.4 Conclusions

In this study, we have established a framework for examining internal energy of any fluid flow governed by the compressible Navier-Stokes equations. Analogous to fluid velocity, a suitable thermodynamic state variable for internal energy is identified ($\phi \sim \sqrt{p}$). It is shown that ϕ is proportional to density-weighted acoustic speed which relates to the internal energy of the system. Defining internal energy in terms of ϕ allows partitioning of the mean internal energy of the flow into the mean field and perturbation field contributions, similar to mean kinetic energy. It is also established that spectral behavior of turbulent internal energy can be rigorously examined using ϕ'. Governing equations for e_m and e_t are derived to identify key internal–kinetic energy interactions. It is anticipated that this framework will be important for analysis and modeling of energy dynamics in high-speed compressible transition and turbulent flows.

3 Study 2: Development and validation of Gas Kinetic Solver For Wall-Bounded Flow

3.1 Introduction

In Study 1, a general analysis of the full equations is performed to identify the prominent interactions between the two components of kinetic and internal energy. In this study we perform a linear stability analysis to develop more insight into the most unstable modes at different Mach numbers. For incompressible flows the linear stability analysis leads to the well known Orr-Sommerfeld equations, the solution of which is the OS mode. Similar linear analysis, developed by Mack (1984), can be performed for compressible flows to identify the most unstable modes and its shape at different Mach number. Due to its simple geometry and intrinsic scientific value, Poiseuille flow has long been used to study wall effects on turbulence and other fluid phenomena. Indeed, incompressible turbulent Poiseuille or channel flow is one of the most widely investigated flows in literature. Therefore, it is reasonable to investigate compressible Poiseuille flow to understand fundamental processes in wall-bounded flows before proceeding to other flow configuration. The objective of this study is to perform a linear stability analysis for wall-bounded flows and identify the effect of Mach number on the most unstable modes. Toward that end we perform the following tasks:

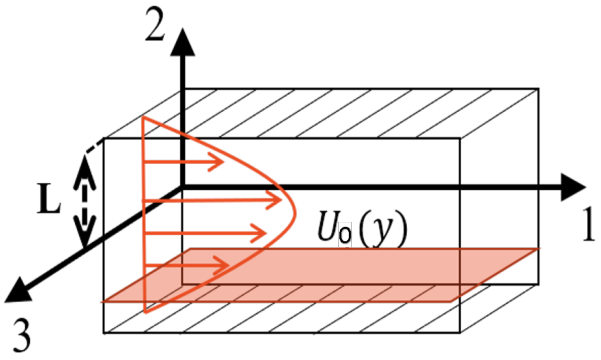

Figure 2: Problem Setup

1. Perform a linear stability analysis and derive the governing equations.
2. Develop a code to solve the above set of equations and identify the most unstable modes and its shape.
3. Verify the code using direct numerical simulations (DNS) of randomly perturbed pressure field.
4. Identify the effect of Mach number on the most unstable modes.

3.2 Compressible linear stability equations

We consider Poiseuille flow as the canonical problem for this analysis as shown in figure 2. The flow variables are non-dimensionalized as follows,

$$\begin{gathered} x_i^* = \frac{x_i}{L}, \quad t^* = \frac{U_0}{L}t, \quad \mu^* = \frac{\mu}{\mu_0}, \quad \kappa^* = \frac{\kappa}{\kappa_0} \\ u_i^* = \frac{u_i}{U_0}, \quad p^* = \frac{p}{p_0}, \quad T^* = \frac{T}{T_0}, \quad \rho^* = \frac{\rho}{\rho_0}, \quad f_b^* = \frac{L}{U_0^2} f_b, \end{gathered} \tag{18}$$

where L is the channel half width, μ_0 is the initial U_0 is the initial centerline velocity, p_0 is the initial uniform pressure, T_0 is the initial uniform temperature, ρ_0 is the initial uniform density and f_b is a constant body force applied to drive the flow. The base flow considered for the stability analysis of full set of linearlized compressible equations is given by,

$$\overline{u_i^*} = (1 - y^{*2}, 0, 0), \quad \overline{p^*} = 1, \quad \overline{T^*} = 1, \quad \overline{\rho^*} = 1, \quad f_b^* = \frac{2}{Re}. \tag{19}$$

The base flow temperature and density are assumed to be uniform. This assumption is validated using DNS simulations for the duration of evolution considered in this paper. Under these assumptions the coefficient of dynamic viscosity (μ) and thermal conductivity (κ) can be considered

constants for the linear stability analysis. Therefore,

$$\mu^* = 1 \quad \text{and} \quad \kappa^* = 1. \tag{20}$$

The flow variables are expressed as a sum of the base field and small perturbations,

$$A^* = \overline{A}^* + A^{*'}. \tag{21}$$

The linearized perturbation equations are derived and can now be expressed as,

$$\frac{\partial \rho^{*'}}{\partial t} + \frac{\partial u_j^{*'}}{\partial x_j} + (1 - y^{*2}) \frac{\partial \rho^{*'}}{\partial x_1} = 0, \tag{22a}$$

$$\frac{\partial u_i^{*'}}{\partial t} + (1 - y^{*2}) \frac{\partial u_i^{*'}}{\partial x_1} - 2y^* u_2^{*'} \delta_{i1} = -\frac{1}{\gamma M^2} \frac{\partial p^{*'}}{\partial x_i} + \frac{2}{Re} \rho^{*'} \delta_{i1} + \frac{1}{Re} \Big[\frac{\partial^2 u_i^{*'}}{\partial x_j \partial x_j} + \frac{1}{3} \frac{\partial^2 u_j^{*'}}{\partial x_i \partial x_j} \Big], \tag{22b}$$

$$\frac{\partial p^{*'}}{\partial t} + (1 - y^{*2}) \frac{\partial p^{*'}}{\partial x_1} + \gamma \frac{\partial u_j^{*'}}{\partial x_j} = \frac{\gamma}{Re\, Pr} \frac{\partial^2 T^{*'}}{\partial x_j \partial x_j} - \frac{4\gamma(\gamma - 1) M^2 y^*}{Re} \Big[\frac{\partial u_1^{*'}}{\partial x_2} + \frac{\partial u_2^{*'}}{\partial x_1} \Big], \tag{22c}$$

$$p^{*'} = \rho^{*'} + T^{*'}, \tag{22d}$$

where $(.)^{*'}$ represents the fluctuations in the flow variables. The dimensionless parameters, Mach number (M), Reynolds number (Re) and Prandtl number (Pr) are defined as,

$$Re = \frac{\rho_0 U_0 L}{\mu_0}, \quad Pr = \frac{\mu_0 c_p}{\kappa_0}, \quad M = \frac{U_0}{\sqrt{\gamma R T_0}}. \tag{23}$$

Normal mode analysis is now performed by representing the flow variables as follows,

$$A^{*'} = A(y) e^{\iota(\alpha x + \beta z - \omega t)}, \tag{24}$$

where A represents velocity components, temperature, density or pressure. The system of equations is reduced to an eigenvalue problem,

$$B\psi = \omega I \psi, \tag{25}$$

where ω is the growth rate for each mode, (α, β) and $\psi = [\hat{u}_1, \hat{u}_2, \hat{u}_3, \hat{\rho}, \hat{T}]^T$ is the mode shape. The general form of eigenvalue problem of the linearized perturbation equations can be referred to from Ramachandran *et al.* (2016). A code is developed to solve the above eigenvalue problem and identify the mode, mode shape and its corresponding growth rate.

3.3 Results

Before analyzing the effect of Mach number on the most unstable modes predicted through linear theory, it is important to verify the linear stability code. As a first step, the code is verified to

	$M_c = 3.0$	$M_c = 4.0$	$M_c = 6.0$
$T\ (K)$	60	60	60
$\rho_0\ (kg\ m^{-3})$	0.04	0.0267	0.02
$U(y;t=0)\ (m\ s^{-1})$	$465.8\left(1-\frac{y^2}{L^2}\right)$	$698.7\left(1-\frac{y^2}{L^2}\right)$	$931.6\left(1-\frac{y^2}{L^2}\right)$

Table 1: Initial base flow conditions for verification with DNS.

Mach Number	CLST [Growth Rate]	DNS
3.0	(5,0) [0.029]	(5,0)
4.5	(3,0) [0.078]	(3,−1)
6.0	(4,0) [0.081]	(4,0)

Table 2: Verification of most unstable mode.

reproduce the OS mode and its shape at low Mach numbers as predicted using the Orr-Sommerfeld equations. Verification at higher Mach numbers is performed using DNS of randomly perturbed pressure field. We consider three Mach numbers for verification as shown in table 1 along with the Initial base flow properties for each Mach number. The Reynolds number is kept constant at $Re = \rho U_0 L/\mu = 93900$ for all simulations.

Random perturbations in the pressure field are initialized as,

$$\frac{p'}{\overline{p}} = A(2r-1), \qquad A = 0.25, \tag{26}$$

where r is a random number uniformly distributed between $[-1,1]$. Simulations are performed using isothermal temperature boundary condition which is also the boundary condition used in the linear stability analysis. We first verify the dominant unstable modes after lapse of initial transience for the three cases. The mode number predicted from linear analysis code is observed to match exactly with the DNS simulations for two cases - $M_c = 3.0$ and $M_c = 6.0$ and is in close proximity for $M_c = 4.5$. We now compare the predicted mode shape for these unstable modes between DNS and CLST. The mode shape through DNS is established using 18 wall normal planes in the flow and by determining the turbulent kinetic energy amplitude of the unstable mode. Figures 3 and

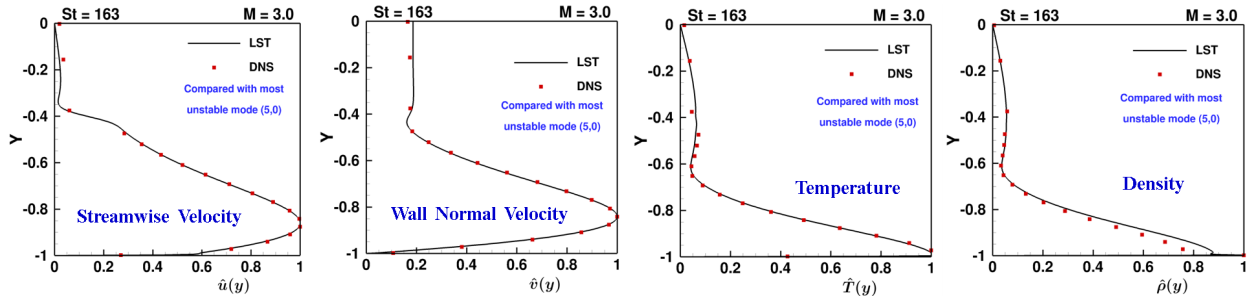

Figure 3: Mode shape comparison between DNS and LST results for $M_c = 3.0$.

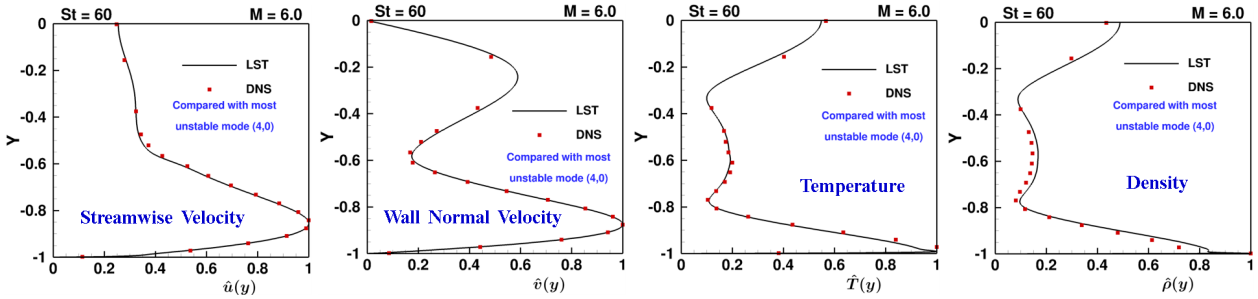

Figure 4: Mode shape comparison between DNS and LST results for $M_c = 6.0$.

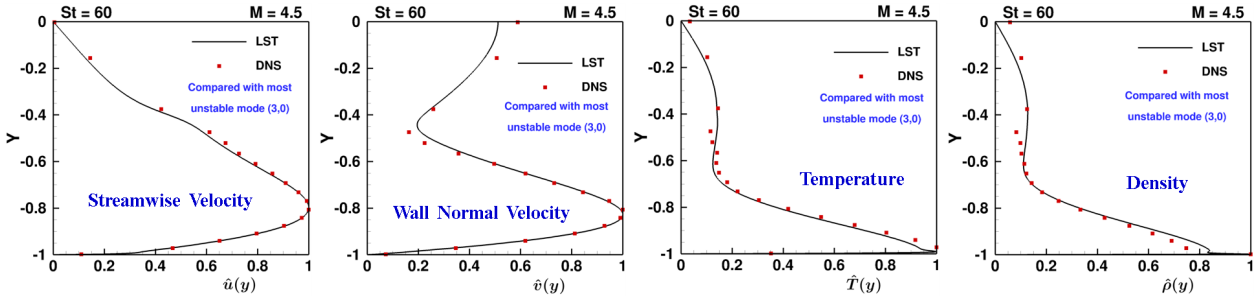

Figure 5: Mode shape comparison between DNS and LST results for $M_c = 4.5$.

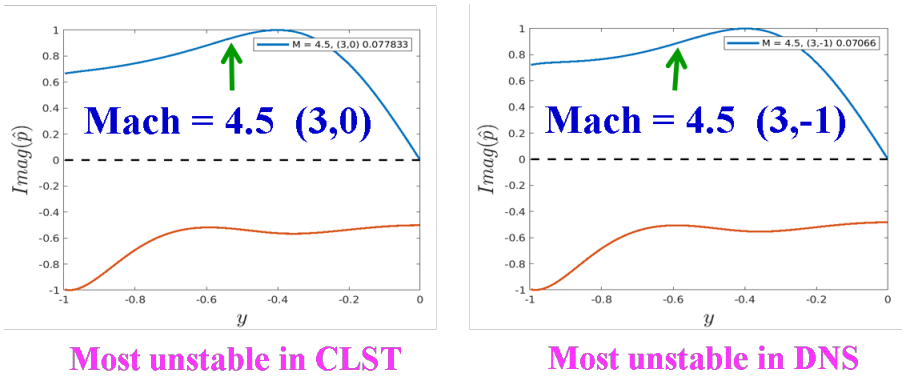

Figure 6: Mode shape comparison between unstable modes $(3, 0)$ and $(3, -1)$ for $M_c = 4.5$.

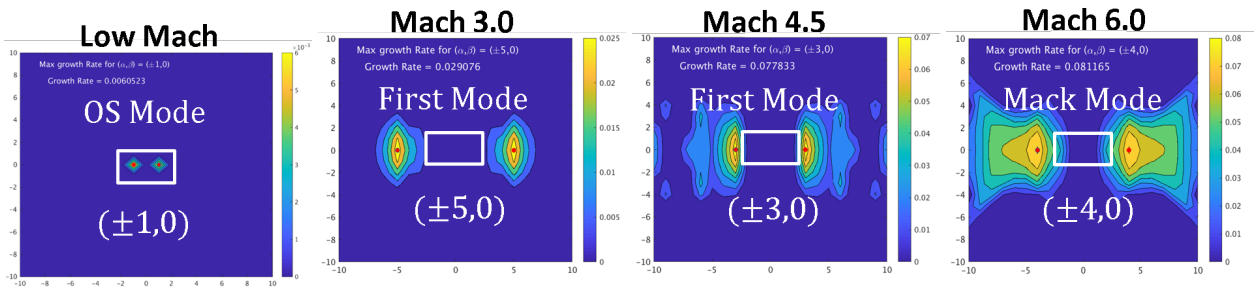

Figure 7: Effect of Mach number on most unstable modes.

4 compare the mode shapes for all flow variables for $M_c = 3.0$ and $M_c = 6.0$ respectively. The mode shapes predicted by LST can be observed to match very well with the DNS results validating the developed linear stability code. We now compare the mode shape for $M_c = 4.5$ for the most unstable mode predicted using linear analysis i.e. $(3,0)$ in figure 5. The mode shape for $(3,0)$ matches well with DNS however, the most unstable mode predicted by DNS is relatively oblique i.e. $(3,-1)$. In figure 6 we compare the mode shape of pressure fluctuations for $(3,0)$ and $(3,-1)$. It can be clearly seen that the mode shapes and growth rates of these modes is very similar. Xie *et al.* (2017) have shown that compressibility suppresses streamwise modes and the suppression effect of compressibility reduces as the obliqueness of the mode increases. Keeping these effects in mind it is understandable that the most unstable mode in DNS is a relatively oblique mode instead of a streamwise mode.

Having validated the code using DNS, we now study the effect of Mach number on the unstable modes predicted through CLST. Figure 7 compares the stability curves across all (α,β) for different Mach numbers with the most unstable mode and its growth rate highlighted on the figure. Even though the number of unstable modes keep increasing as we increase the Mach number, the low wavenumbers (highlighted within the white box) are stabilized for high Mach number cases which were originally most unstable for low Mach numbers. It can therefore, be concluded that low wavenumbers are stabilized due to the velocity - pressure interactions at high Mach numbers. This effect can be characterized using the effective gradient Mach number (Xie *et al.* 2017), defined as

$$M_g^e = \frac{S}{\kappa a}\cos\beta \quad \text{where} \quad S = \frac{\partial \overline{U}}{\partial y}, \tag{27}$$

as the relevant parameter. M_g^e is inversely proportional to wavenumber causing high wavenumbers to experience a low effective gradient Mach number thereby reducing compressibility suppression. It also includes the effect of obliqueness since streamwise modes experience the highest M_g^e whereas the spanwise modes are unaffected. These inferences will prove useful in understanding the effect of velocity-pressure interactions on the nonlinear processes. The variation in the most unstable mode number as a function of Mach number is left as future work.

3.4 Conclusions

In this study, we have performed a compressible linear stability analysis and developed a code to solve eigenvalue problem. The code is validated by comparing the most unstable mode and its shape with DNS of randomly perturbed pressure field at various Mach numbers. Initial random pressure perturbations lead to development of the most unstable mode (mode number and shape) predicted by CLST. It is also established that low wavenumbers are stabilized for compressible cases affirming the relevance of the effective gradient Mach number, M_g^e for compressible flows. These insights in the linear regime are important before analyzing the effect of compressibility on key

nonlinear processes such as scale to scale cascade of energy.

4 Non-linear Breakdown in hypersonic wall bounded flow

Pressure undergoes a transformative change as the Mach number increases from incompressible to compressible regime. In incompressible flows, pressure is a Lagrange multiplier governed by the Poisson equation and its sole purpose is to maintain a divergence-free velocity field. At high Mach numbers pressure is a thermodynamic state variable and its evolution is governed by energy conservation and state equations. Emergence of wave-like character in the pressure field engenders a dilatational velocity component at high Mach numbers. Flow-thermodynamic interactions enabled by the dilatational field become significant and profoundly affect the flow field. The pressure field performs work on the velocity field via the pressure-dilatation interaction leading to kinetic-internal energy exchange. Compressibility effects in the linear stability regime and fully developed turbulence have been reasonably well investigated in literature. Study of nonlinear development of velocity perturbations is critically important for understanding and modeling breakdown toward turbulence in hypersonic boundary layers. Despite recent progress, many important fundamental aspects of nonlinear processes - specifically those due to the change in the action of pressure - are not well understood. It is well known that dilatational fluctuations exhibit vastly different spectral transfer characteristics than solenoidal velocity field. Further, the effect of energy exchange between kinetic and internal forms on spectral evolution is not established in wall-bounded flows. Recall that in incompressible turbulence, kinetic energy is conserved in the nonlinear spectral transfer process. It is therefore reasonable to expect that transient spectral evolution in incompressible and compressible flows can potentially be significantly different. Thus motivated, the goal of this study is to examine the nonlinear spectral evolution in high-speed wall-bounded flows with a focus on pressure effects. Toward this end, we undertake the following tasks:

1. Analyse the governing equations to establish the key role of pressure and dilatation on the nonlinear evolution of perturbations.

2. Perform direct numerical simulations of perturbation evolution (linear and early nonlinear stages) in Poiseuille flows at incompressible and compressible Mach numbers.

3. Examine the effect of pressure-dilatation on internal energy evolution and kinetic energy spectral growth at different Mach numbers.

4. Examine the spectral growth in different wall-normal regions of high Mach number flow as a function of local pressure-dilatation level. Then the contrast between the spectral evolution in high and low speed wall bounded flows can be clearly established.

4.1 Analysis

Energy equipartition: Turbulent kinetic energy has two components, energy in solenoidal fluctuations and that in dilatational fluctuations. Only the dilatational component of turbulent kinetic energy interacts with internal energy. Previous studies of compressible shear flows have shown dilatational field to be dominated by the wall-normal component of velocity perturbations. The inviscid evolution of the wall normal component of turbulent kinetic energy ($k_{(2)} = \overline{\rho u_2'' u_2''}/2$), which is approximately the dilatational kinetic energy, is given by:

$$\frac{\partial k_{(2)}}{\partial t} + \frac{\partial (k_{(2)} \tilde{U}_j)}{\partial x_j} + \frac{\partial}{\partial x_j}\left[\frac{1}{2}\overline{\rho u_j'' u_2'' u_2''} + \overline{p' u_2''}\delta_{j2}\right] = -\overline{\rho u_2'' u_j''}\frac{\partial \tilde{U}}{\partial x_2} + \overline{p'\frac{\partial u_2''}{\partial x_2}} - \overline{u_2''}\frac{\partial \overline{p}}{\partial x_2}. \tag{28}$$

The inviscid evolution of normalized pressure-variance $[\overline{p'p'}/(2\gamma\overline{p})]$ which is the potential energy incumbent in the pressure fluctuations is given by:

$$\begin{aligned}\frac{1}{2\gamma\overline{p}}\left[\frac{\partial(\overline{p'p'})}{\partial t} + \frac{\partial(\overline{p'p'}\tilde{U}_k)}{\partial x_k} + \frac{\partial}{\partial x_k}\left(\overline{p'p'u_k''}\right)\right] &= -\frac{\overline{p'u_k''}}{\gamma\overline{p}}\frac{\partial \overline{p}}{\partial x_k} - \overline{p'\frac{\partial u_k''}{\partial x_k}} \\ &\quad -\left(1-\frac{1}{2\gamma}\right)\frac{1}{\overline{p}}\left[\overline{p'p'}\frac{\partial \tilde{U}_k}{\partial x_k} + \overline{p'p'\frac{\partial u_k''}{\partial x_k}}\right].\end{aligned} \tag{29}$$

Since the velocity gradients in the wall-normal component in planar shear flows are dominant the following approximation can be made:

$$\overline{p'\frac{\partial u_k''}{\partial x_k}} \sim \overline{p'\frac{\partial u_2''}{\partial x_2}}. \tag{30}$$

It is evident that pressure-dilatation leads to a harmonic exchange between normalized pressure-variance and the wall-normal component of turbulent kinetic energy $k_{(2)}$. Due to the harmonic nature of this interaction, equipartition of energy between these two energy forms can be expected.

Relevant parameter: The evolution of turbulent kinetic energy (k) in compressible flows in eq. (7) shows three major inviscid mechanisms that influence the evolution of k as: production $\left(P_k = -\overline{\rho u_i'' u_j''}\frac{\partial \tilde{U}_i}{\partial x_j}\right)$, pressure-dilatation mechanism $\left(\overline{p'd''} = \overline{p'\frac{\partial u_k''}{\partial x_k}}\right)$ and pressure work on mean of Favre fluctuations $\left(\overline{u_k''}\frac{\partial \overline{p}}{\partial x_k}\right)$. In the early nonlinear regime, the last term is likely to be small compared to production and pressure-dilatation. Therefore, P_k and $\overline{p'd''}$ remain as the two important inviscid mechanisms affecting the evolution of turbulent kinetic energy and spectral transfer. We propose that the pressure-dilatation to production ratio is the important non-dimensional parameter that governs the degree of compressibility effect on kinetic energy evolution. Thus,

$$\begin{aligned}|\overline{p'd''}| &> |P_k| \quad => \quad \text{Large compressibility effects,} \\ |\overline{p'd''}| &< |P_k| \quad => \quad \text{Small compressibility effects.}\end{aligned} \tag{31}$$

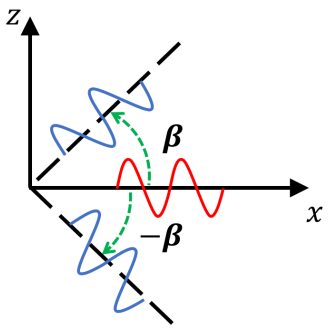

Figure 8: Initial perturbations

4.2 Problem Setup

This study can be considered an extension of Xie *et al.* (2017) which examines the linear mechanisms. Thus, we use the same flow configuration and parameter range of investigation. The computational domain is a rectangular box of dimension $8L \times 2L \times 4.64L$ and the setup can be seen in figure 2. Temporal simulations are performed and the evolution is considered in dimensionless shear time defined as:

$$St = x^* = \frac{U_0 t}{L}. \tag{32}$$

The base flow is perturbed with a triad of disturbances of as shown in figure 8 following the studies of Sivasubramanian and Fasel (2015). The disturbances are superposed on different wall-normal profiles. We consider the following initial perturbation profiles:

1. The incompressible Orr-Sommerfeld (OS) perturbation profile which generates Tollmien-Schlichting (TS) waves leading to first mode instability.

2. A dilatation-free arbitrary perturbation profile given by,

$$\begin{aligned} u_1' &= U_0 \sin\left(\pi \frac{x_2}{L}\right) \sin\left(2\pi \frac{x_1 + x_3 \tan\beta}{L_{x_1}}\right), \\ u_2' &= U_0 \left(\frac{2L}{L_{x_1}}\right) \left[\cos\left(\pi \frac{x_2}{L}\right) + 1\right] \cos\left(2\pi \frac{x_1 + x_3 \tan\beta}{L_{x_1}}\right), \\ u_3' &= 0, \end{aligned} \tag{33}$$

   where L_{x_1} is the domain length in the streamwise direction and L is the half channel width. We will refer to this profile as the arbitrary initial profile.

3. A hybrid profile which is a linear superposition of OS and the arbitrary profiles. This profile will be referred to as combined initial profile.

4. The most energetic Mack mode (at $M_c = 6.0$) determined using the linear analysis code developed in previous study. This profile will be referred to as Mack mode profile.

Case	Initial Profile	Initial Spectra	Perturbation amp. (% of U_0)	Initial Turbulence Intensity (I_0)
1	OS	$\beta = (-60°, 0°, 60°)$	(1.33, 1.33, 1.33)	0.9%
2	OS	$\beta = (-60°, 0°, 60°)$	(0.83, 0.83, 0.83)	0.56%
3	OS	$\beta = (-60°, 0°, 60°)$	(0.33, 0.33, 0.33)	0.22%
4	OS	$\beta = (-60°, 0°, 60°)$	(0.1, 3.8, 0.1)	1.48%
5	OS	$\beta = (-60°, 0°, 60°)$	(0.1, 1.0, 0.1)	0.39%
6	OS	$\beta = (-45°, 0°, 45°)$	(1.33, 1.33, 1.33)	0.9%
7	Arbitrary	$\beta = (-60°, 0°, 60°)$	(0.95, 0.95, 0.95)	0.9%
8	Arbitrary	$\beta = (-60°, 0°, 60°)$	(0.33, 0.33, 0.33)	0.31%
9	Combined	$\beta = (-60°, 0°, 60°)$	(0.6, 0.6, 0.6)	0.7%
10	Combined	$\beta = (-60°, 0°, 60°)$	(0.15, 0.15, 0.15)	0.18%
11	Mack Mode	$\beta = (-60°, 0°, 60°)$	(1.12, 1.12, 1.12)	0.9%
12	Mack Mode	$\beta = (-60°, 0°, 60°)$	(0.16, 0.16, 0.16)	0.12%

Table 3: Simulations performed.

The initial turbulence intensity is maintained at $I_0 = 0.9\%$ for the cases considered for detailed discussion in this study. We define the initial turbulence intensity (I_0) as,

$$I_0 = \frac{\sqrt{2k_0/\rho_0}}{U_0} \tag{34}$$

where, k_0 is the initial turbulent kinetic energy, ρ_0 is the initial density and U_0 is the initial centerline velocity.

4.3 Results

Since the results for the first three profiles have already been submitted in previous reports, we will present only the results for the Mack mode profile. The objective here is to perform a quantitative comparison of kinetic energy spectral evolution between low and high Mach number cases. The comparison of OS mode evolution at low and high Mach numbers presents useful insight. However, that comparison does not account for the fact that OS mode is not the most unstable perturbation at high speeds. We propose that a meaningful comparison should examine the evolution of most unstable mode specific to each Mach number. Therefore, here we will compare and contrast the spectral evolution of the perturbation field initialized with OS mode for low Mach number and the Mack mode for high Mach number. The most unstable Mack mode is determined from linear stability theory as explained in the previous study. In each simulation, a triad (one streamwise and two oblique) of the appropriate perturbation modes are superposed on the background field at the initial time – see table 3. Then the evolution of various flow quantities are examined.

We first examine the kinetic energy evolution in the two high Mach number simulations (Cases 11 and 12) in Figure 9. The kinetic energy of the higher initial perturbation intensity simulation

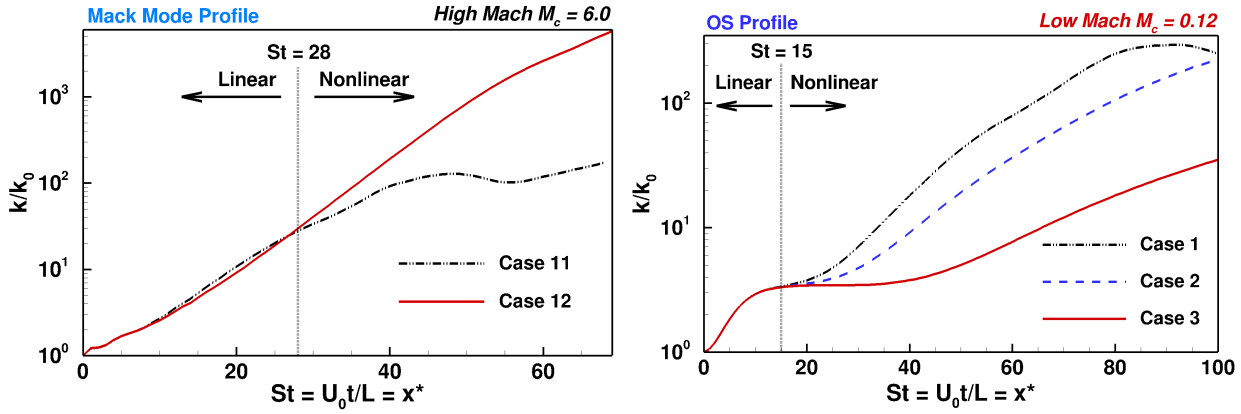

Figure 9: Volume averaged turbulent kinetic energy evolution for different perturbation intensities with Mack mode initial profile at high Mach number and OS initial profile at low Mach number. Initial perturbations with $\beta = 0°, \pm 60°$ are equally energized.

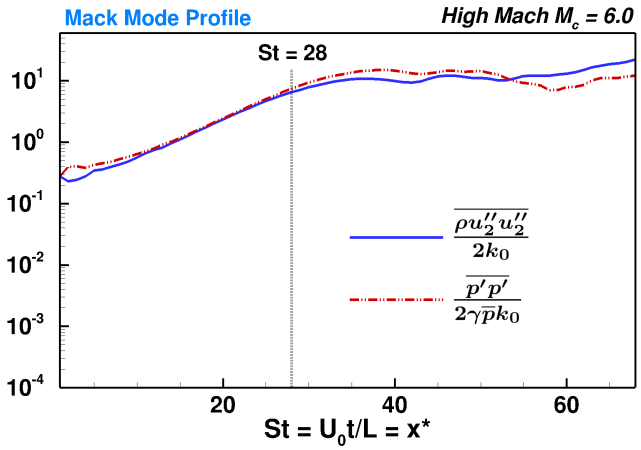

Figure 10: Evolution of volume averaged $\overline{\rho u_2'' u_2''}$ and $\overline{p'p'}/\gamma\overline{p}$ for Mack mode initial profile.

(Case 11) deviates from that of the lower perturbation intensity case at about $St \sim 28$. The onset of nonlinearity of the low Mach number case with OS initial profile (Case 1) happens around $St \sim 15$. This reiterates that compressibility leads to an extended linear regime. Interestingly, upon the onset of nonlinearity, the growth rate of turbulent kinetic energy of the initial high intensity simulation (Case 11) is lower than that of the low intensity case (Case 12). This suggests that the new scales of motion produced by nonlinear spectral transfer may be more stable than the initial Mack mode.

We also investigate the volume-averaged wall-normal component of turbulent kinetic energy ($k_{(2)}$) and the normalized pressure variance ($\overline{p'p'}/2\gamma\overline{p}$) for Case 11. Figure 10 shows the two energies to be nearly equal. This reaffirms the fact that pressure-dilatation continues to enforce energy equipartition.

As previously established, pressure-dilatation to production ratio is a key feature that influences spectral evolution in compressible turbulence. As we expect the compressibility effect to depend on distance from the wall, we examine pressure-dilatation levels at different wall-normal planes. The three planes considered are - near wall plane ($y/L = -0.86$), intermediate plane ($y/L = -0.73$) and

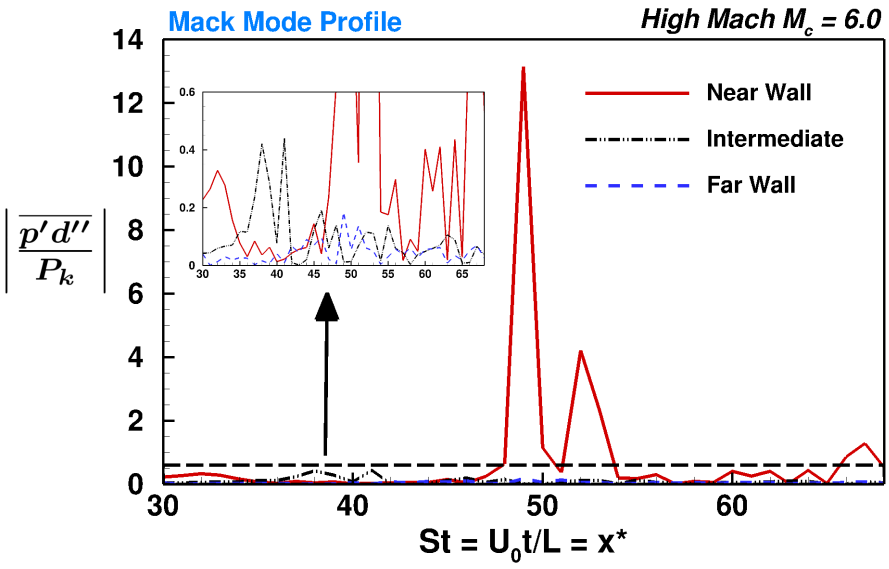

Figure 11: Comparison of pressure-dilatation ($\overline{p'd''}$) to production (P_k) ratio at different $y-$planes for $M_c = 6.0$ initialized with Mack mode profile.

a far-wall plane ($y/L = -0.5$). Figure 11 shows the temporal evolution of $|\overline{p'd''}/P_k|$ at each of these planes. It can be inferred from the figure that (i) the near wall plane experiences the highest levels of $|\overline{p'd''}/P_k|$ ratio and (ii) the relative importance of pressure-dilatation decreases with increasing wall distance. The near and intermediate locations experience moderate levels of dilatation effects within $St \in [30, 48]$ and at later times ($St > 48$), the near-wall plane experiences very high levels of pressure-dilatation.

We now proceed to compare the spectral evolution at different wall-normal distances in high (Case 11) and low (Case 1) Mach number Poiseuille flows. It must be noted that the wavenumber values and mode profiles are very different for the two cases. The normalized (by streamwise length, L_x) wavenumber of the most unstable mode is unity at low Mach number and four at high Mach number. The wavenumbers associated with the oblique modes are a little higher than the streamwise ones due to the nature of initialization. Figures 12 and 13 compare the spectral evolution of high and low Mach number cases at different times. The initial spectra at all wall-normal distances are identical. For the low Mach number case with OS initial profile (figure 13) the spectra continue to be nearly identical for all three planes throughout the period of time considered. The high Mach number Poiseuille flow presents a completely different scenario (figure 12). The spectra on the three planes are reasonably similar until about $St \sim 50$. At later stages, however, vast differences in the spectra are evident. The differences between the spectra arise at about the time when the pressure-dilatation to production ratio grows to large values. The near-wall plane, with the highest values of $|\overline{p'd''}/P_k|$, clearly exhibits the least amount of kinetic energy and the narrowest spectrum. The kinetic energy level and spectral width of the intermediate plane are both larger than than those of near-wall plane. As was shown earlier, the intermediate plane experiences moderate levels of pressure-dilatation. The far-wall plane, with little or no pressure-dilatation,

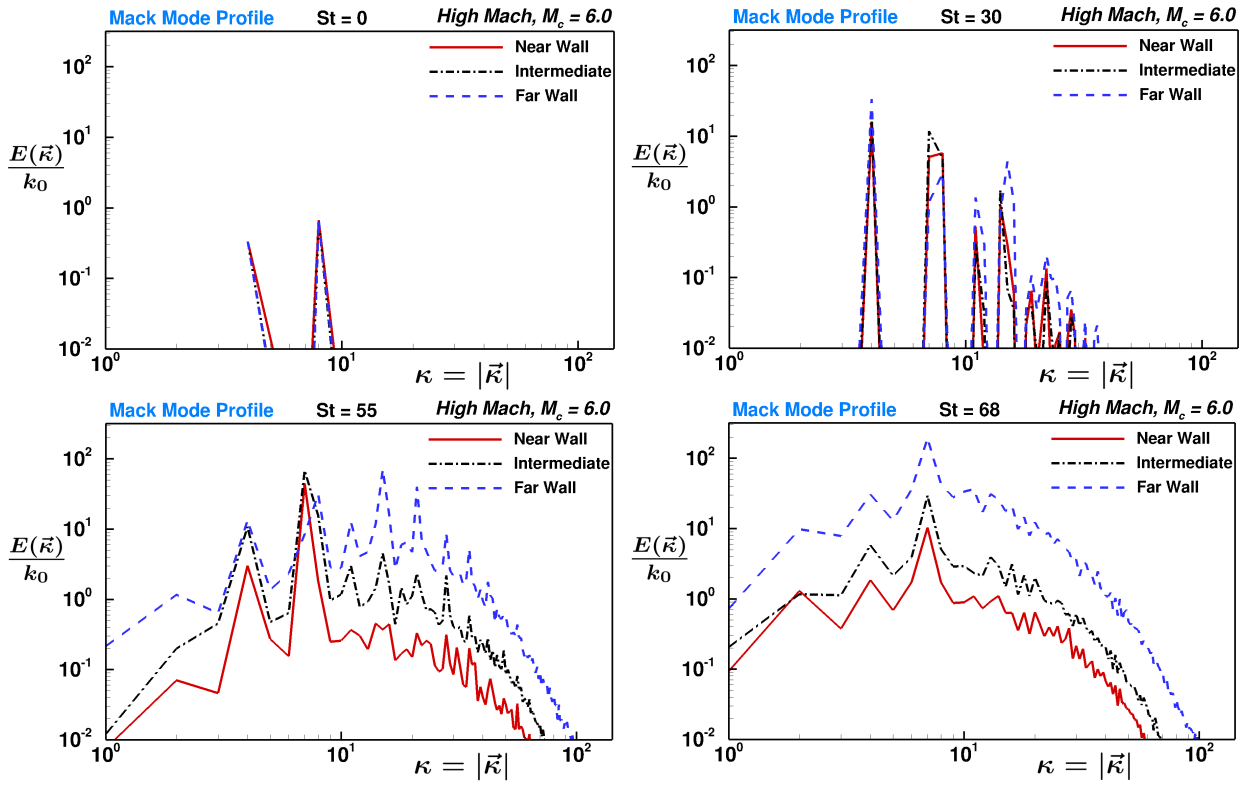

Figure 12: Evolution of turbulent kinetic energy line spectra for high Mach flow initialized with Mack mode profile at near wall ($y/L = -0.86$), intermediate ($y/L = -0.73$) and far wall ($y/L = -0.5$) planes.

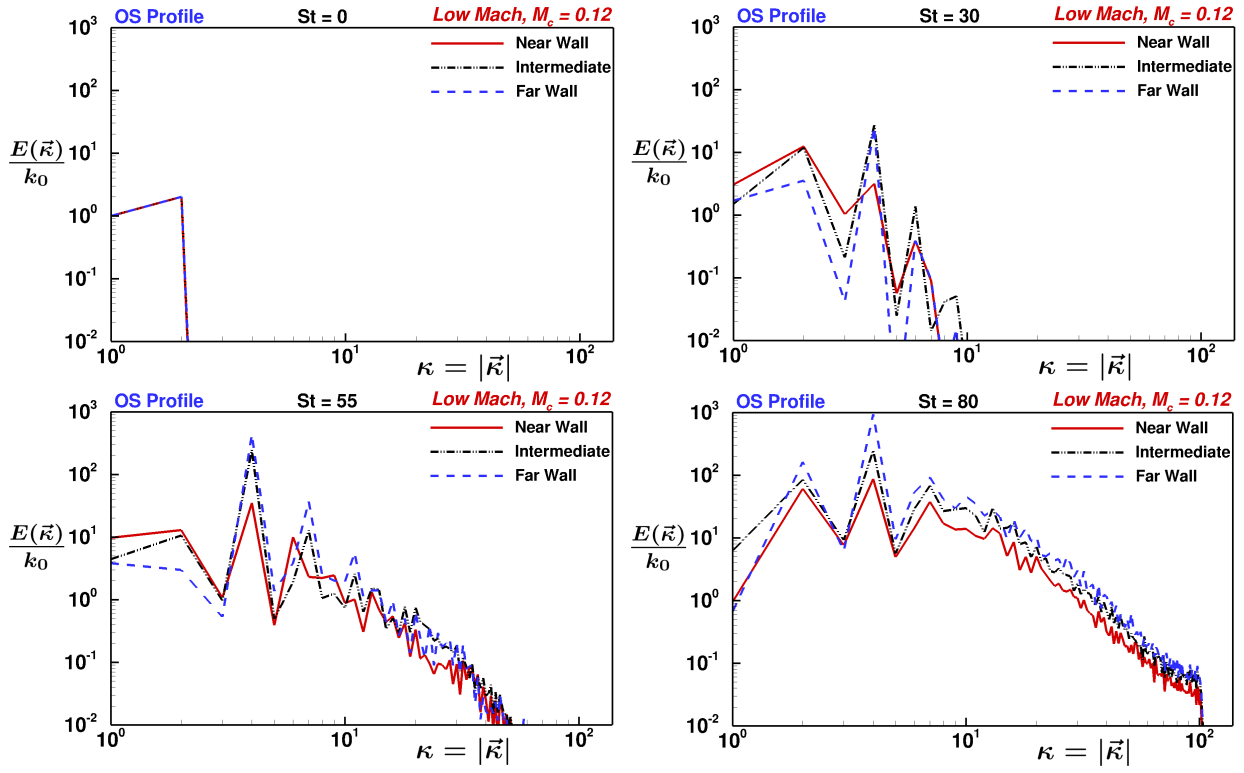

Figure 13: Evolution of turbulent kinetic energy line spectra for low Mach flow initialized with OS profile at near wall ($y/L = -0.86$), intermediate ($y/L = -0.73$) and far wall ($y/L = -0.5$) planes.

exhibits the largest value of kinetic energy and the widest spectrum. These findings clearly imply that in high-speed Poiseuille flow, the nonlinear effects are onset at different rates at different wall-normal locations. Specifically, the spectral growth is slowest near the wall and is progressively faster away from the wall. On the contrary, the onset nonlinear processes are reasonably independent of wall-normal distance at low speeds.

5 Conclusions

Compressibility profoundly affects the nonlinear evolution of the perturbation field in high Mach number flows. Emergence of dilatational fluctuations leads to the onset of kinetic–internal energy exchange via pressure-dilatation mechanism. This study contrasts the nonlinear stages of turbulent kinetic energy growth, flow-thermodynamic interactions and spectral growth in compressible and incompressible wall-bounded shear flows. The key inferences from this study are summarized below.

1. The wall-normal component of the perturbation field is shown to be dominantly dilatational in nature. The turbulent kinetic energy of wall-normal fluctuations is nearly equipartitioned with normalized pressure-variance in the linear and nonlinear regimes in the overall flow field (volume-averaged sense), at each $y-$plane and even at each wavenumber. In high speed flows, equipartition is achieved regardless of the initial profile of perturbations.

2. Pressure-dilatation to production ($|\overline{p'd''}/P_k|$) ratio is identified as the important non-dimensional parameter which characterizes the degree of compressibility effects on turbulent kinetic energy evolution.

3. When $|\overline{p'd''}| > |P_k|$:

   (a) The growth rate of turbulent kinetic energy is highly suppressed relative to a similar low Mach case.

   (b) The spectral transfer rate is significantly reduced leading to slow down in spectrum growth at high speeds.

4. When $|\overline{p'd''}| < |P_k|$, effect of compressibility on turbulent kinetic energy growth and spectral transfer of energy remains insignificant. The flow field evolves similar to a comparable low speed flow.

The above inferences are important for understanding and modeling the laminar-turbulent boundary layer transition process for high-speed flows. The slowdown in spectral energy transfer may cause an extended linear and nonlinear phase of the perturbation field evolution. The rate of spectral growth can also be reduced and breakdown to turbulence maybe delayed for compressible flows.

6 Publications and Presentations

Journal Articles

1. A. Mathematical framework for analysis of internal energy dynamics and spectral distribution in compressible turbulent flows. *A Mittal, SS Girimaji.* **Physical Review Fluids** 4 (4), 042601, 2019 (This paper was selected as the Editor's pick, an honor given to only 10% of accepted papers).

2. Effect of pressure-dilatation on energy spectrum evolution in compressible turbulence. DS Praturi, SS Girimaji. Physics of Fluids 31 (5), 055114, 2019.

3. Nonlinear evolution of perturbations in high Mach number wall-bounded flow: Pressure-dilatation effects. Mittal, Ankita; Girimaji, Sharath (submitted)

The work conducted under the grant also resulted in 4 conference presentations.